5-2023

Inhibitors of Human ENO2 are Potent Anti-Trypanosomal Agents

Danielle LaVigne

Inhibitors of Human ENO2 are Potent Anti-Trypanosomal Agents

Departmental Honors Thesis in Biochemistry

Danielle LaVigne

Dr. James Morris

Table of Contents

Abstract

Kinetoplastid parasite infections remain a global health burden. Here, we have characterized inhibitors of an essential *Trypanosoma brucei* glycolytic enzyme, enolase (*Tb*ENO). We anticipate *Tb*ENO inhibitors will be potent anti-trypanosomals, as *T. brucei* relies on glycolysis for ATP production in the blood of infected mammals. Additionally, the phosphonate enolase inhibitors being considered are well-tolerated in mammals, suggesting their potential in developing novel therapeutics for kinetoplastid infections. *Tb*ENO was cloned into the bacterial expression vector, pQE-30, and the heterologously-expressed protein was purified by nickel affinity and assayed in a coupled enzyme assay. Enzyme activity paralleled the abundance of a ~45 kDa protein, consistent with the predicted size of *Tb*ENO. Preliminary inhibition assays have demonstrated that phosphonate-based enolase inhibitors could be promising leads for blocking the glycolytic pathway in the pathogen. For example, (1-hydroxy-2-oxopyrrolidin-3-yl) phosphonic acid (deoxy-SF2312) was a potent enzyme inhibitor (IC50 value of 0.60 ± 0.23 μM), while larger ring-bearing variants were less potent. Molecular docking simulations supported this supposition, as larger ring-bearing variants were predicted to have lower binding affinities. The inhibitory potency and anti-trypanosomal activity of these compounds suggest they are promising therapeutic leads for future development.

Acknowledgments

Thank you to Dr. Florian Muller (MD Anderson) for providing phosphonate inhibitors and to Dr. Jillian Milanes (Clemson University) for her support on this project. Thank you to Clemson Creative Inquiry for their support as well. Work was supported in part by the US National Institutes of Health Center for Biomedical Excellence (COBRE) grant under award number P20GM146584.

I. Background

Lifecycle of the Trypanosome

The African trypanosome, *Trypanosoma brucei*, is the protozoan parasite responsible for African sleeping sickness in humans and nagana in livestock animals. The lifecycle of the trypanosome is complex. The tsetse fly transmits these parasites to humans or other mammals through a bite as the flies feed on mammalian blood. The CDC outlines this process (Figure 1). Parasites are injected as metacyclic trypomastigotes, where they enter the bloodstream and can travel throughout the body. They multiply by binary fission in various bodily fluids and circulate the blood during the acute phase. The parasites can then be transferred to a new tsetse fly whenever it bites an infected human and ingests the trypomastigotes. The trypanosomes then transform into their procyclic forms in the midgut of the fly and multiply, again by binary fission. These eventually leave the midgut and transform into epimastigotes, where they multiply in the salivary gland of the fly. There they transform into the metacyclic form. The cycle can start over again when this fly bites another human or animal (CDC, 2022).

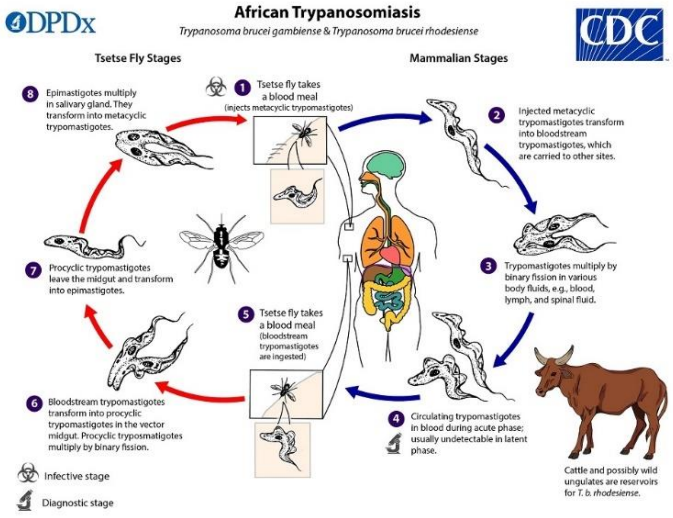

Figure 1. The complex lifecycle of the African trypanosome. The lifecycle consists of different organisms, making up the tsetse fly stages and the mammalian stages (CDC, 2022).

Stages of Infection

Infection occurs in two stages: a first stage, where the parasites are found in the blood and lymphatic system, followed by a second stage, after the parasites invade the central nervous system (Kenyon College, 2018). Some common symptoms of African sleeping sickness include lethargy, confusion, and wasting as the parasite enters the brain. If left untreated, the disease is fatal within weeks to months of being infected (Kenyon College, 2018). Treatments vary based on the progression and stages of the disease. Fexinidazole, a potent oral anti-trypanosomal drug, has proven very useful in the treatment of human disease (Kande Betu Kumesu et al., 2022). However, concerns over possible resistance to this lone effective drug support the identification of additional therapeutics. Additionally, fexinidazole will not be used in animals over concerns of generating resistance (Kande Betu Kumesu et al., 2022). Animal disease is a multi-billion dollar problem in sub-Saharan Africa that threatens human health by impacting food availability.

Glycolytic Pathway of *T. brucei*

Glucose metabolism is critical for *T. brucei*, as the bloodstream form (BSF) parasite uses glycolysis as its sole source of ATP in the glucose-rich environment of the host blood. The glycolytic enzyme *Tb*ENO converts 2-phosphoglycerate into phosphoenolpyruvate for the downstream production of pyruvate, which is secreted from the cell (Figure 2). The *Tb*ENO genome predicts the protein to have 431 residues in its structure, resulting in a size of 46.6 kDa (da Silva Giotto et al., 2003). It is reported that *Tb*ENO is only found in the cytosol of cells, and

the structure of enolase is well conserved (Hannaert et al., 2003). This protein has been well annotated in the RCSB protein data bank.

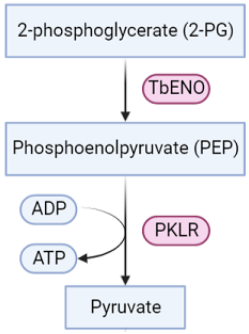

Figure 2. Glycolytic pathway of *T. brucei* leading to the secretion of pyruvate.

II. Aims

Since glucose metabolism is critical for *T. brucei*, this reaction is a promising therapeutic target (Figure 3). Recently, phosphonate inhibitors of human enolase 2 (*Hs*ENO2) have been developed for the treatment of glioblastoma multiforme, which is an aggressive brain tumor. This project involves testing these agents against *T. brucei* enolase (*Tb*ENO). Humans have multiple enolases as compared to *T. brucei*, which has one obvious ortholog in the genome. Additionally, the phosphonate enolase inhibitors being considered are well-tolerated in mammals, suggesting their potential in developing novel therapeutics for kinetoplastid infections.

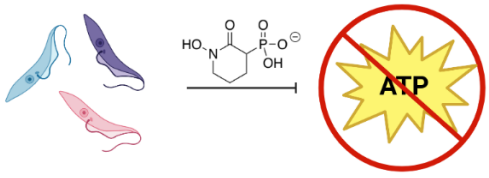

Figure 3. Aims of the project. Enolase inhibitors are hypothesized to inhibit the glycolytic pathway of trypanosomes, thus inhibiting their production of ATP, suggesting therapeutic leads.

III. Materials and Methods

Chemicals and Reagents

Glucose-6-phosphate dehydrogenase, β-nicotinamide adenine dinucleotide phosphate (NADP +), and phosphoenolpyruvate (PEP) were purchased from Alfa Aesar (Haverhill, MA). β-nicotinamide adenine dinucleotide (NADH), adenosine triphosphate (ATP), and dimethyl sulfoxide (DMSO) were from Fisher Scientific (Pittsburgh, PA). The phosphonate ENO inhibitors (1-hydroxy-2-oxopyrrolidin-3-yl) phosphonic acid (deoxy-SF2312), (1-hydroxy-2-oxopiperidin-3-yl) phosphonic acid (HEX), and (1-hydroxy-2-oxoazepan-3-yl) phosphonic acid (HEPTA), were synthesized as described by Lin et al. (Lin et al., 2020).

Protein Purification

The full-length open reading frame was amplified from *Trypanosoma brucei brucei* genomic DNA (a 427 strain). It was then cloned into the bacterial expression vector pQE-30 (Qiagen, Hilden, Germany). This plasmid was transformed into M15pREP cells, and protein expression was induced with 1mM isopropyl-b-d-1-thiogalactopyranoside (IPTG) overnight at 37 C. This enolase was purified using a nickel affinity column using Ni-NTA agarose (Qiagen, Hilden, Germany), as described in the methods of Sharlow et al. (Sharlow et al., 2010).

Protein purification was assessed by SDS PAGE. Briefly, protein samples were mixed with 5X cracking buffer (5g glycerol, 1g SDS, 1ml β-mercaptoethanol, 1ml 1M Tris pH 6.8, 1ml 1% Bromophenol blue, ddH_2O to 10ml) and then resolved on a 12% polyacrylamide gel at 120 V for 120 minutes. Gels were stained with Coomassie Blue overnight and destained with a mixture of methanol, acetic acid, and water by gentle shaking for 2 hours (Figure 4).

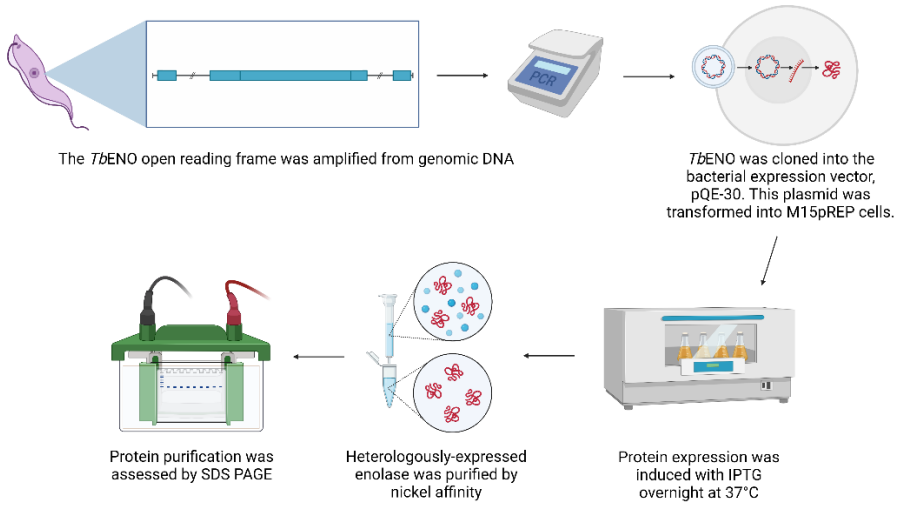

Figure 4. A schematic overview of the methods for the protein purification of *T. brucei* enolase.

Enolase Assay

To assess the activity of the recombinant enolase, the protein was mixed with 1X enolase buffer (100 mM HEPES, pH 8.0, 3.3 mM $MgSO_4$), 0.4 mM NADH, 1.75 mM ADP, 1 U of pyruvate kinase/lactate dehydrogenase, and 120 mM KCl and added in triplicate to a black 96-well plate. The reaction was initiated with 3.75 mM 2-PG added to each well, besides the last well, which was used as a control where the volume was adjusted with water. The assay utilizes the pathway to measure the oxidation of NADH, which was monitored at OD_{340} on a Biotek Synergy H1 plate reader every 20 seconds for 4 minutes (Figure 5). The assay measures the coupled fluorescence of this reaction. Addition of LDH allows the oxidation of NADH, converting the pyruvate into lactate.

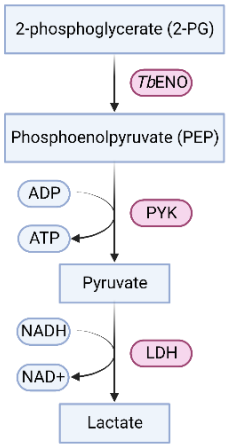

Figure 5. Pathway of inhibition assay, measuring the oxidation of NADH.

For the inhibition assay, serial dilutions of the compound being tested were made in DMSO and added in triplicate to a black 96-well plate. Enolase buffer (100 mM HEPES, pH 8.0, 3.3 mM $MgSO_4$), 0.4 mM NADH, 1.75 mM ADP, 1 U of pyruvate kinase/lactate dehydrogenase, and 120 mM KCl were mixed with the enolase enzyme to create an enzyme master mix. This was added to the wells and incubated for 15 minutes at room temperature. The substrate, 3.75mM 2-PG, was added to all wells except wells used as a control that lacked substrate. Assays were scored on a Biotek Synergy H1 microplate reader, and kinetic analyses were performed using Prism 9.0 (GraphPad Software, San Diego, CA) using the Michaelis-Menten model to calculate IC50 values (Figure 6).

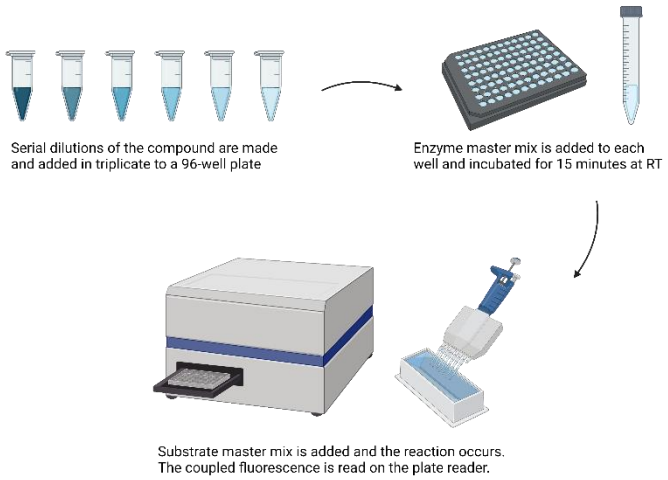

Figure 6. Steps of inhibition assay for enolase.

Docking Simulations

The chemical structures of SF2312, deoxy-SF2312, HEX, POMHEX, and HEPTA were drawn with ChemOffice professional 19 suite (PerKinElmer, Waltham, MA), and three-dimensional (3D) structures were generated with VeraChem Vconf (VerChem LLC, Germantown, MD). The 3D crystal structure of *Tb*ENO (PDB 2PTY) was retrieved from the RCSB protein data bank (Navarro, 2007). The protein was then prepared for the docking analysis by first removing co-crystallized ligands, heteroatoms, and water molecules using Pymol Molecular Graphics 2.0 (Schrödinger LLC, New York, NY). The optimized ligands and the protein were further prepared using AutoDock Tools (The Scripps Research Institute, La Jolla, CA) to convert all structures into pdbqt formats. A grid box was prepared around the region of the active site of the protein. The molecular docking studies were carried out *in vacuo* with AutoDock vina using specific docking parameters and scoring functions reported in the literature (Trott & Olson, 2009).

IV. Results

Purification of *Tb*ENO

After purification, a band consistent with the 46.6 kD mass predicted for the *Tb*ENO 429 amino acid primary sequence was noted (Figure 7). The larger band in the elutions may be a chaperone, as it is similar in size to that protein. Overall, the sample is seen to become purer after the initial flow through and washes (Figure 7).

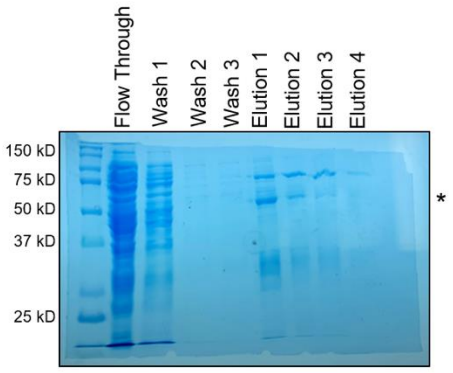

Figure 7. Coomassie stained gel showing purification of *Tb*ENO. Astrisk (*) shows band correlating to the predicated size of *Tb*ENO.

Inhibitor Quantification

Assays were performed in concentrations with a dilution factor of 2 to try to create a curve to calculate IC50 values. IC50 stands for inhibitory concentration. The IC50 value is the concentration of the inhibitor that is needed to inhibit the pathway by 50%. A smaller IC50 value means a compound is a more potent inhibitor. One compound, POMHEX, was tested using a range of 0.625-20µM to calculate the IC50, which was found to be around 2.83µM (Figure 8).

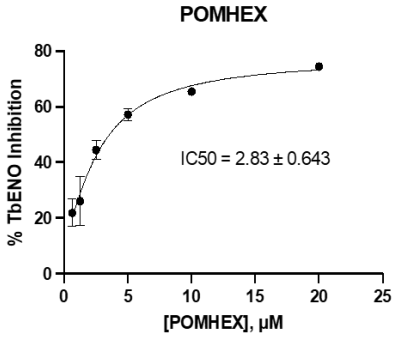

Figure 8. Example of IC50 curve and calculation from compound POMHEX.

While POMEX is one example, other phosphonate-bearing inhibitors were also tested (Table 1). The *Tb*ENO IC50 values were compared to human enolase 2 (*Hs*ENO2) and the bloodstream form (BSF) of *T. brucei*. EC50 stands for effective concentration. This is very similar to IC50 but instead refers to the inhibition of cell growth or viability. In this setting, IC50 typically refers to *in vitro* work, and EC50 is used for more *in vivo* studies. A value of >10 means it's not potent enough to calculate IC50, which is simply the standard.

Compound	Structure	*TbENO* IC_{50} (µM)	*Hs*ENO2 IC_{50} (µM)	*T. brucei* BSF EC_{50} (µM)
SF2312	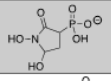	XX ± XX	0.63 ± 0.01	>10
POMSF	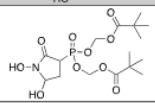	XX ± XX	>10	0.45 ± 0.10
HEX	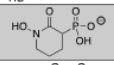	2.1 ± 1.1	0.36 ± 0.04	>10
BenzylHEX	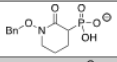	>10	>10	>10
POMHEX	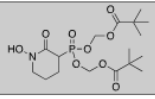	2.8 ± 0.64	>10	0.61 ± 0.08
Deoxy-SF2312	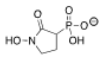	0.60 ± 0.23	0.10 ± 0.04	>10
Benzyl- deoxy-SF2312	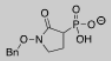	>10	>10	>10
HEPTA	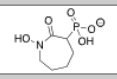	>10	5.8 ± 0.88	> 10
Benzyl-HEPTA	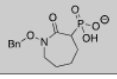	XX ± XX	>10	>10

Table 1. Phosphonate ENO2 inhibitors inhibit *Tb*ENO and have anti-trypanosomal activity.

Molecular Docking

A collaboration with Dr. Daniel Whitehead's lab (Clemson University) led to the performance of molecular docking simulations. The docking score solves the potential energy change when the protein and ligand come together. This means that a very negative score corresponds to a strong binding, and a less negative or even positive score corresponds to a weak or non-existing binding. SF2312 and deoxy-SF2312 bind to the active site of *Tb*ENO with binding affinities of -7.2 and -6.8 kcal/mol, respectively, whereas HEPTA has a lower binding affinity of -4.8 kcal/mol (Figure 9).

A)

Compound	Docking Score
HEX	-7.5
deoxy-SF2312	-6.8
HEPTA	-4.8
POMHEX	-6.6
SF2312	-7.2
Bno-HEX	not docked

B)

Figure 9. A) Docking scores (kcal/mol) simulated for each inhibitor. **B)** A model of *Tb*ENO bound to PEP (Navarro et al., 2007).

Sequence Comparisons

The genomic sequence of *Tb*ENO was compared to the sequences of *Naegleria fowleri*, a brain-eating amoeba, enolase (*Nf*ENO) and *Hs*ENO2 (Figure 10). The *Tb*ENO sequence is closer to *Hs*ENO2 (63%) but still shares similarities with *Nf*ENO (46%). Importantly, *Tb*ENO shares residues with *Hs*ENO2 that are necessary for interactions with phosphonate inhibitors, including Arg372 (in *Hs*ENO2) that is required to form a salt bridge with the compound (Lin et al., 2020).

	*Tb*ENO
*Nf*ENO	46 (62)
*Hs*ENO2	63.0 (78)

Numbers are % identity and % positives
*Nf*ENO (NfTy_054390)
*Hs*ENO2 (*ENOG_Human*, P09104)

Figure 10. Sequence comparisons of enolases. Analyses were performed in BLAST (https://blast.ncbi.nlm.nih.gov/Blast.cgi) using default parameters.

Purification Optimization

When trying to purify more samples of *Tb*ENO, a more pure sample was produced as indicated by the lack of other bands in the elutions (Figure 11). There is also more protein as seen with the darker bands (Figure 11). Unfortunately, the activity of *Tb*ENO has not been as high as previously seen in earlier experiments. This gel was run with retransformed *Tb*ENO as it was hypothesized that the retransformation would help find activity. Current activity is about ten times lower than seen in initial studies.

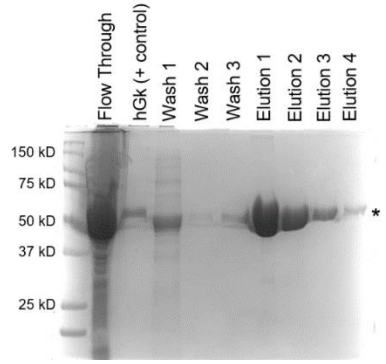

Figure 11. Recent gel from purification after retransformation. Human glycerol kinase was used as a positive control.

V. Discussion and Conclusions

*Tb*ENO was successfully partially purified as a soluble active protein, as indicated by the ~45kD band after purification (Figure 7). Deoxy-SF2312 (1-hydroxy-2-oxopyrrolidin-3-yl phosphonic acid) was a potent enzyme inhibitor (IC50 value of 0.60 ± 0.23 µM), while larger ring-bearing variants were less potent (Table 1). Molecular docking simulations supported this supposition, as larger ring-bearing variants were predicted to have lower binding affinities (Figure 9). This is due to the bulky nature of the larger ring-bearing variants not being well tolerated in the active site of *Tb*ENO. Other inhibitors were found to have IC50 values indicating the potency of compounds in halting the glycolytic pathway. Overall, phosphonate ENO2 inhibitors inhibit *Tb*ENO and have anti-trypanosomal activity (Table 1).

Upon further analysis, we can determine that both SF2312 and deoxy-SF2312 adopt a binding conformation similar to PEP bound to the active site of *Tb*ENO (Figure 9). Whereas HEPTA binding affinity is reduced (-4.8 kcal/mol) with the seven-membered HEPTA ring not being as well tolerated in the active site. This difference distinguishes *Tb*ENO from other enolases, including *Nf*ENO and *Hs*ENO2, which had similar binding patterns for these inhibitors (Milanes et al., in preparation). The *Tb*ENO sequence is closer to *Hs*ENO2 but still shares similarities with *Nf*ENO (Figure 10). It is interesting to note that POMHEX binds *Tb*ENO well but doesn't bind *Nf*ENO. This may be due to greater tolerance of the POM-protecting group with *Tb*ENO. That POM group cannot fit in the active site of *Nf*ENO but is modeled to reasonably fit into the active site of *Tb*ENO. It is likely that once the compound is taken up by the cell, cellular esterases cleave off the POM group. The observed docking scores and the inhibitory effect of POMHEX on *Tb*ENO further shows the variability and flexibility of the *Tb*ENO active site compared with other enolases, as previously reported.

Additional purifications were seen to be optimized by the presence of a purer and more abundant sample (Figure 11). However, it is unclear why the new samples are not active. Retransformation resulted in a new sample with new expression, which was predicted to result in more active protein. Before continuing with testing more inhibitors, the activity must be found. It is likely that one of the reagents isn't great and affecting the outcome of the reaction. Each old reagent should be tested individually with new reagents in an assay to determine the source of the faulty reagent.

Overall, *Tb*ENO was successfully partially purified as a soluble active protein, as indicated by the purification gels. Potent phosphonate ENO2 inhibitors, including HEX derivatives, were identified as seen in the inhibition assays. These compounds are being further characterized as these inhibitors are promising therapeutic leads for kinetoplastid infections, specifically African sleeping sickness. The addition of potential new therapeutics will allow for the treatment of both humans and other mammals and reduce the risk of resistance.

VI. Future Direction

The future direction of this project includes purifying more active enolase to continue testing new inhibitors. We are also interested in solving some of the kinetic information, such as the Km for 2-PG and potentially pH sensitivity. And lastly, we would want to move *in vivo* with rodent infection studies. These studies would entail infecting rats with trypanosomes and then treating them with the compound either intraperitoneal or intravenously. These compounds will need to cross the blood-brain barrier for the later-stage disease when the parasites are in the brain.

References

Centers for Disease Control and Prevention. (2022, February 16). CDC - african trypanosomiasis. Centers for Disease Control and Prevention. Retrieved from https://www.cdc.gov/parasites/sleepingsickness/index.html

Kenyon College. (2018). African sleeping sickness: Trypanosome Invasion mechanism. microbewiki. Retrieved from https://microbewiki.kenyon.edu/index.php/African_Sleeping_Sickness:_Trypanosome_Invasion_Mechanism

Kande Betu Kumesu, V., Mutombo Kalonji, W., Bardonneau, C., Valverde Mordt, O., Ngolo Tete, D., Blesson, S., Simon, F., Delhomme, S., Bernhard, S., Nganzobo Ngima, P., Mahenzi Mbembo, H., Fina Lubaki, J.-P., Lumeya Vuvu, S., Kuziena Mindele, W., Ilunga Wa Kyhi, M., Mandula Mokenge, G., Kaninda Badibabi, L., Kasongo Bonama, A., Kavunga Lukula, P., … Tarral, A. (2022). Safety and efficacy of oral fexinidazole in children with gambiense human African trypanosomiasis: A Multicentre, single-arm, open-label, phase 2–3 trial. *The Lancet Global Health*, *10*(11). https://doi.org/10.1016/s2214-109x(22)00338-2

da Silva Giotto, M. T., Hannaert, V., Vertommen, D., Navarro, M. V., Rider, M. H., Michels, P. A. M., Garratt, R. C., & Rigden, D. J. (2003). The crystal structure of Trypanosoma brucei enolase: Visualisation of the inhibitory metal binding site III and potential as target for selective, irreversible inhibition. Journal of Molecular Biology, 331(3), 653–665. https://doi.org/10.1016/s0022-2836(03)00752-6

Hannaert, V., Albert, M.-A., Rigden, D. J., Theresa da Silva Giotto, M., Thiemann, O., Garratt, R. C., Van Roy, J., Opperdoes, F. R., & Michels, P. A. (2003). Kinetic characterization, structure modelling studies and crystallization of Trypanosoma brucei enolase. *European Journal of Biochemistry, 270*(15), 3205–3213. https://doi.org/10.1046/j.1432-1033.2003.03692.x

Images created with BioRender.com

Lin, Y.-H., Satani, N., Hammoudi, N., Yan, V. C., Barekatain, Y., Khadka, S., Ackroyd, J. J., Georgiou, D. K., Pham, C.-D., Arthur, K., Maxwell, D., Peng, Z., Leonard, P. G., Czako, B., Pisaneschi, F., Mandal, P., Sun, Y., Zielinski, R., Pando, S. C., … Muller, F. L. (2020). An enolase inhibitor for the targeted treatment of eno1-deleted cancers. *Nature Metabolism, 3*(1), 122–122. https://doi.org/10.1038/s42255-020-00335-x

Sharlow, E. R., Lyda, T. A., Dodson, H. C., Mustata, G., Morris, M. T., Leimgruber, S. S., Lee, K.-H., Kashiwada, Y., Close, D., Lazo, J. S., & Morris, J. C. (2010). A target-based high throughput screen yields trypanosoma brucei hexokinase small molecule inhibitors with antiparasitic activity. *PLoS Neglected Tropical Diseases, 4*(4). https://doi.org/10.1371/journal.pntd.0000659

Navarro, M. V. A. S., Rigden, D. J., Garratt, R. C., & Dias, S. M. G. (2007). Crystal structure of the T. brucei enolase complexed with pep. https://doi.org/10.2210/pdb2pty/pdb

Trott, O., & Olson, A. J. (2009). Autodock Vina: Improving the speed and accuracy of docking with a new scoring function, efficient optimization, and multithreading. *Journal of Computational Chemistry*. https://doi.org/10.1002/jcc.21334

Jillian E. Milanes, Elijah M. Harding, Victoria C. Yan, Florian Muller, Samuel Kwain, Kerrick C. Rees, Brian Dominy, Daniel C. Whitehead, Steven W. Millward, Madison Weiss, Bart Staker, Ashley Moseman, Xiang Zhang, Xipeng Ma, Audriy Jebet, Xinmin Yin, & James C. Morris. Enolase inhibitors as therapeutic leads for Naegleria fowleri infection. [Manuscript in preparation]